Chemical Science

ROYAL SOCIETY OF CHEMISTRY

EDGE ARTICLE

View Article Online
View Journal | View Issue

Cite this: *Chem. Sci.*, 2024, **15**, 16618

All publication charges for this article have been paid for by the Royal Society of Chemistry

Incorporation of 2D pyreneammonium iodide for enhancing the efficiency and stability of perovskite solar cells†

Zhongquan Wan, *[ab] Yuanxi Wang,[a] Hui Lu,[b] Runmin Wei,[b] Haomiao Yin,[a] Huaibiao Zeng,[b] Muhammad Azam,[a] Junsheng Luo*[ab] and Chunyang Jia *[ab]

Despite the excellent performance of three-dimensional (3D) perovskite-based solar cells (PSCs), their poor stability under moisture and heating conditions limits their commercial application. To address this issue, a new pyreneammonium iodide (named TAPPyI), in which the pyrene-based compound 4,4′,4″,4‴-(1,8-dihydropyrene-1,3,6,8-tetrayl)tetraaniline (named TAPPy) acts as the 2D cation, is introduced into 3D perovskite precursor solution for forming a 2D/3D heterostructured perovskite, which improves the quality of the perovskite film and enhances the stability of the perovskite film against moisture and heating. The planar pyrene endows TAPPyI with good charge transport properties, while the iodide on the arylamine side group effectively passivates the perovskite defects, thereby suppressing non-radiative recombination losses. Finally, the power conversion efficiency (PCE) of the TAPPyI-modified PSC is increased from 20.51% in the reference PSC to 22.73%. Furthermore, the stability of the TAPPyI-modified PSC is greatly improved, retaining 86% of the initial PCE after 360 hours in an environment of 85 °C and 85% humidity (ISOS-D-3), whereas the reference PSC only retains 2%. This work demonstrates that the conjugated planar molecule as a 2D cation to construct a 2D/3D heterostructured perovskite, which combines the good stability of 2D perovskite with the excellent carrier transport properties of 3D perovskite, can greatly enhance the efficiency and stability of PSCs.

Received 19th July 2024
Accepted 10th September 2024

DOI: 10.1039/d4sc04819a

rsc.li/chemical-science

1. Introduction

Organic–inorganic hybrid three-dimensional (3D) perovskite solar cells (PSCs) have attracted widespread attention due to their high absorption coefficient,[1] low exciton binding energy,[2] long carrier diffusion length[3] and tunable bandgap.[4] In recent years, although the power conversion efficiency (PCE) has exceeded 26%,[5] the poor stability under moisture and heating conditions has restricted their commercial application and large-scale production.[6] Previous studies have shown that the chemical composition at the grain boundaries of 3D perovskite films is mainly terminated by iodide ions or ammonium ions.[7] The intrinsic instability of ammonium ions, such as methylammonium cations (MA^+), makes them prone to release from the film under moisture and heating conditions, leading to defects like uncoordinated Pb^{2+}, which subsequently affect the photovoltaic performance and stability of PSCs.[2,8]

To address the aforementioned issues, researchers have begun to study low-dimensional PSCs, such as two-dimensional (2D) PSCs.[9] In fact, 2D perovskite is derived from the original 3D structure by inserting large-volume organic cations (such as *n*-butylammonium and 2-phenylethylammonium) between the anionic layers,[10] resulting in high environmental stability.[11] Due to the substitution of traditional smaller organic cations (such as FA^+ and MA^+) with larger organic cations in 2D perovskites, they exhibit greater moisture and heat stability.[12] Therefore, in order to simultaneously utilize the good stability of 2D perovskites and the high efficiency of 3D perovskites, 2D/3D heterostructured perovskites have been developed.[13] However, although 2D/3D heterostructured perovskites exhibit improved stability, most 2D organic cations are insulating, which is not conducive to charge transfer and limits further improvements in the performance of PSCs.[10]

Therefore, compounds containing large planar conjugated aromatic moieties have aroused great interest among researchers because they can exhibit sufficiently high intrinsic charge carrier mobility.[14] It is well known that planar conjugated aromatic molecules tend to undergo strong intermolecular interactions through π–π stacking, forming ordered structures that often exhibit good charge transport properties.[15]

[a]*National Key Laboratory of Electronic Films and Integrated Devices, School of Integrated Circuit Science and Engineering, University of Electronic Science and Technology of China, 611731 Chengdu, P. R. China. E-mail: zqwan@uestc.edu.cn; luojs@uestc.edu.cn; cyjia@uestc.edu.cn*

[b]*Shenzhen Institute for Advanced Study, University of Electronic Science and Technology of China, 518110 Shenzhen, P. R. China*

† Electronic supplementary information (ESI) available. See DOI: https://doi.org/10.1039/d4sc04819a

In particular, some pyrene-based compounds have been successfully applied in organic light-emitting diodes and PSCs due to their excellent charge transport performance and heat stability (glass transition temperatures exceeding 300 °C).[16] Furthermore, previous research has shown that pyrene derivatives containing arylamine or thienyl side groups can effectively passivate perovskite defects, thereby enhancing the efficiency of PSCs.[17]

In this work, a new pyreneammonium iodide (named TAPPyI), in which the pyrene-based compound 4,4′,4″,4‴-(1,8-dihydropyrene-1,3,6,8-tetrayl)tetraaniline (named TAPPy) acts as the 2D cation, is introduced into 3D perovskite precursor solution for forming a 2D/3D heterostructured perovskite. The quality of the 2D/3D heterostructured perovskite film has been significantly improved, with an increase in grain size and a smoother and denser surface. Due to the hydrophobicity of the pyrene and aromatic ring of TAPPyI, as well as the formation of a more stable 2D perovskite structure, it exhibits high moisture and heat stability. Owing to the presence of iodine atoms with lone pair electrons, TAPPyI can act as a Lewis base to passivate Pb^{2+} defects in perovskite films, and can also interact with I ions in the perovskite lattice to compensate for halide vacancies. Meanwhile, the four arylammonium groups on TAPPyI can interact with Pb^{2+} defects *via* hydrogen bonding, reducing trap density and enhancing charge transport capability. Based on the above-mentioned advantages, the performance of the PSC modified with TAPPyI has been greatly improved, with PCE increasing from 20.51% to 22.73%, and its stability against moisture and heating has also been greatly enhanced.

2. Results and discussion

The synthesis and mass spectrometry of TAPPyI are shown in Fig. S1 and S2,† respectively. The TAPPyI modified PSC was prepared by adding TAPPyI to the perovskite precursor solution and the PSC structure diagram and cross-sectional SEM images are shown in Fig. 1a and c, respectively. Compared with the control PSC (Fig. S3†), the grains of the perovskite layer in the TAPPyI modified PSC are significantly larger and denser. To confirm the formation of the 2D/3D heterostructured perovskite after introducing TAPPyI (conceptual diagram shown in Fig. 1b), X-ray diffraction (XRD) patterns were analyzed. As illustrated in Fig. 1d and S4,† there are two main types of diffractions in the patterns. The first type of diffraction peaks located at 14.12°, 28.40°, and 31.82° correspond to the (110), (220), and (310) crystal planes of the 3D perovskite, indicating good crystal orientation of the prepared 3D perovskite. The second type of diffraction peaks at 6.0°, 9.1°, and 11.6° correspond to the crystal structure of the 2D perovskite, indicating the formation of a 2D perovskite structure within the 3D perovskite lattice in the TAPPyI-modified perovskite film. And the intensity of these diffraction peaks of 2D perovskite increases with the concentration of TAPPyI (Fig. S5†). Notably, after TAPPyI modification, the peak intensity corresponding to PbI_2 (at 12.7°) is significantly reduced, indicating a greater conversion of PbI_2. This could be due to the enhanced moisture and heat stability of the 2D perovskite, which prevents the escape of cations such as MA^+ and FA^+ and reduces the moisture uptake of PbI_2 during spin coating.

The influence of TAPPyI on the surface morphology of perovskite films was studied using SEM and AFM. As shown in Fig. 1e and f, the introduction of TAPPyI increases the grain size of perovskite and makes the perovskite film surface denser. In Fig. 1h and i and S6,† compared to the reference perovskite film (18.1 nm), the root mean square (RMS) roughness of the TAPPyI-modified perovskite film (16.8 nm) is slightly reduced, indicating a smoother film surface. The better quality of the TAPPyI-modified perovskite film is mainly attributed to two reasons: (1) the auxiliary crystallization effect of the 2D perovskite. The formation of 2D perovskite between the surface and grains of the 3D perovskite facilitated better film arrangement, improving the crystallization of the perovskite film, thereby enhancing grain size and smoothness. (2) Lewis acid–base interaction between TAPPyI and uncoordinated Pb^{2+}. TAPPyI effectively passivates uncoordinated Pb^{2+} defects in the perovskite film through Lewis acid–base interaction, delaying the crystallization process of perovskite and thus promoting the formation of a more uniform film. It is noteworthy that a smooth perovskite film ensures close contact with the charge transport layer and suppresses the formation of unfavorable phases and interface defects, thereby promoting effective charge extraction at the interface, reducing charge accumulation and recombination, which contributes to an improved fill factor (FF). In addition, as shown in Fig. 1g, the addition of TAPPyI is beneficial for enhancing the visible light absorption of perovskite, which is attributed to the better quality of the perovskite film. In a word, the addition of TAPPyI to the 3D perovskite precursor solution forms a 2D/3D heterostructured perovskite, significantly improving film quality, which is beneficial for improving the PCE and stability of PSCs.

In addition to forming 2D perovskite, TAPPyI can also passivate defects. The structure of TAPPyI was optimized and its electrostatic surface potential (ESP) was calculated, as shown in Fig. 2a and b. From Fig. 2b, it can be seen that the high electronegativity of TAPPyI is mainly located near the iodide atoms, which suggests that TAPPyI can strongly coordinate with Pb^{2+}. Additionally, the adsorption energy of TAPPyI on the perovskite surface was studied using first-principles calculations. As shown in Fig. 2c, TAPPyI was placed on the perovskite surface, and the binding energy with the perovskite surface is −2.81 eV after structure optimization, which indicates that TAPPyI has the feasibility of passivating phase boundary defects.

Furthermore, the passivation mechanism of TAPPyI on perovskite defects was studied. As depicted in Fig. 2d and e, a typical uncoordinated Pb^{2+} defect (Pb–Pb dimer) was placed on the terminal of the perovskite (001) crystal plane to simulate deep-level defect states on the perovskite surface, and TAPPyI was positioned on the perovskite surface. Subsequently, the charge density difference between the TAPPyI and the Pb^{2+} defect was computed to visualize the process of charge transfer, as shown in Fig. 2f and g. When TAPPyI is placed on the (001) crystal plane of perovskite, the charge accumulation on the surface of the Pb–Pb dimer is inhibited. Clearly, the I atom on

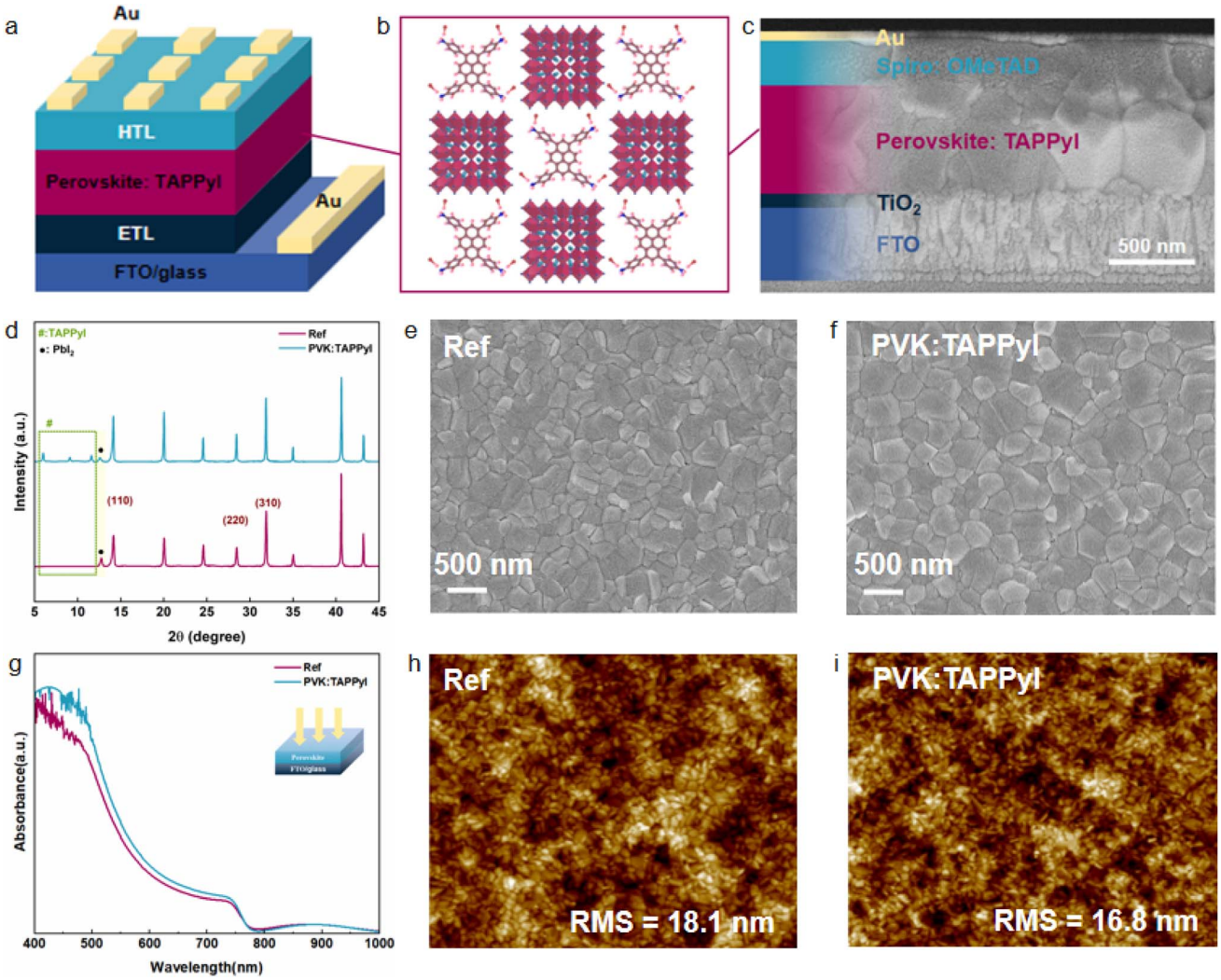

Fig. 1 Characteristics of the perovskite films before and after 0.50 mg per mL TAPPyI modification. (a) Cross-sectional diagram of the PSC; (b) conceptual diagram of the 2D/3D composite structure perovskite; (c) cross-sectional SEM image of the PSC; (d) XRD spectra of the perovskite film before and after modification; (e) surface morphology of the perovskite film without TAPPyI doping; (f) surface morphology of the perovskite film with TAPPyI doping; (g) UV-vis spectra of the perovskite film before and after modification; (h) surface AFM image of the reference perovskite film; (i) surface AFM image of the perovskite film after modification.

TAPPyI donates electrons to the Pb–Pb dimer, causing a shift in defect states, demonstrating the effective passivation of defects at perovskite grain boundaries by TAPPyI. In addition, comparing the partial density of states (PDOS) before and after the passivation of perovskite grain boundaries as shown in Fig. 2h and i, it was found that the deep level defect state caused by the Pb–Pb dimer on the perovskite surface was eliminated after TAPPyI interacted with the defect surface, which is beneficial for reducing the non-radiative recombination centers at the perovskite grain boundaries and improving the carrier transport capacity.

To verify the interaction between TAPPyI and perovskite, X-ray photoelectron spectroscopy (XPS) was used to characterize the perovskite films before and after TAPPyI modification, as shown in Fig. 3a. The binding energies of Pb $4f_{5/2}$ and Pb $4f_{7/2}$ in the reference perovskite film are 143.40 eV and 138.60 eV, respectively. After introducing TAPPyI into the perovskite film, the binding energies of Pb $4f_{5/2}$ and Pb $4f_{7/2}$ shift towards lower binding energy directions to 143.30 eV and 138.50 eV, respectively. In Fig. S7,† the binding energies of I $3d_{3/2}$ and I $3d_{5/2}$ are 618.17 eV and 629.57 eV, respectively. After introducing TAPPyI, the binding energies of I $3d_{3/2}$ and I $3d_{5/2}$ change to 618.07 eV and 629.47 eV, respectively. The negative shift in the Pb peak position is due to the binding of I in TAPPyI with uncoordinated Pb^{2+}, where Pb^{2+} gains electrons, leading to a decrease in Pb binding energy, thus passivating the uncoordinated Pb^{2+} defects. Meanwhile, TAPPyI can also interact with I ions in the perovskite lattice to compensate for halogen vacancies, leading to negative migration of I. In addition, it was found that after the introduction of TAPPyI, the two peaks of N 1s in the perovskite film shifted from 399.47 eV and 401.45 eV to lower binding energies of 399.37 eV and 401.05 eV, respectively (Fig. S8†), which may be caused by the hydrogen bonding

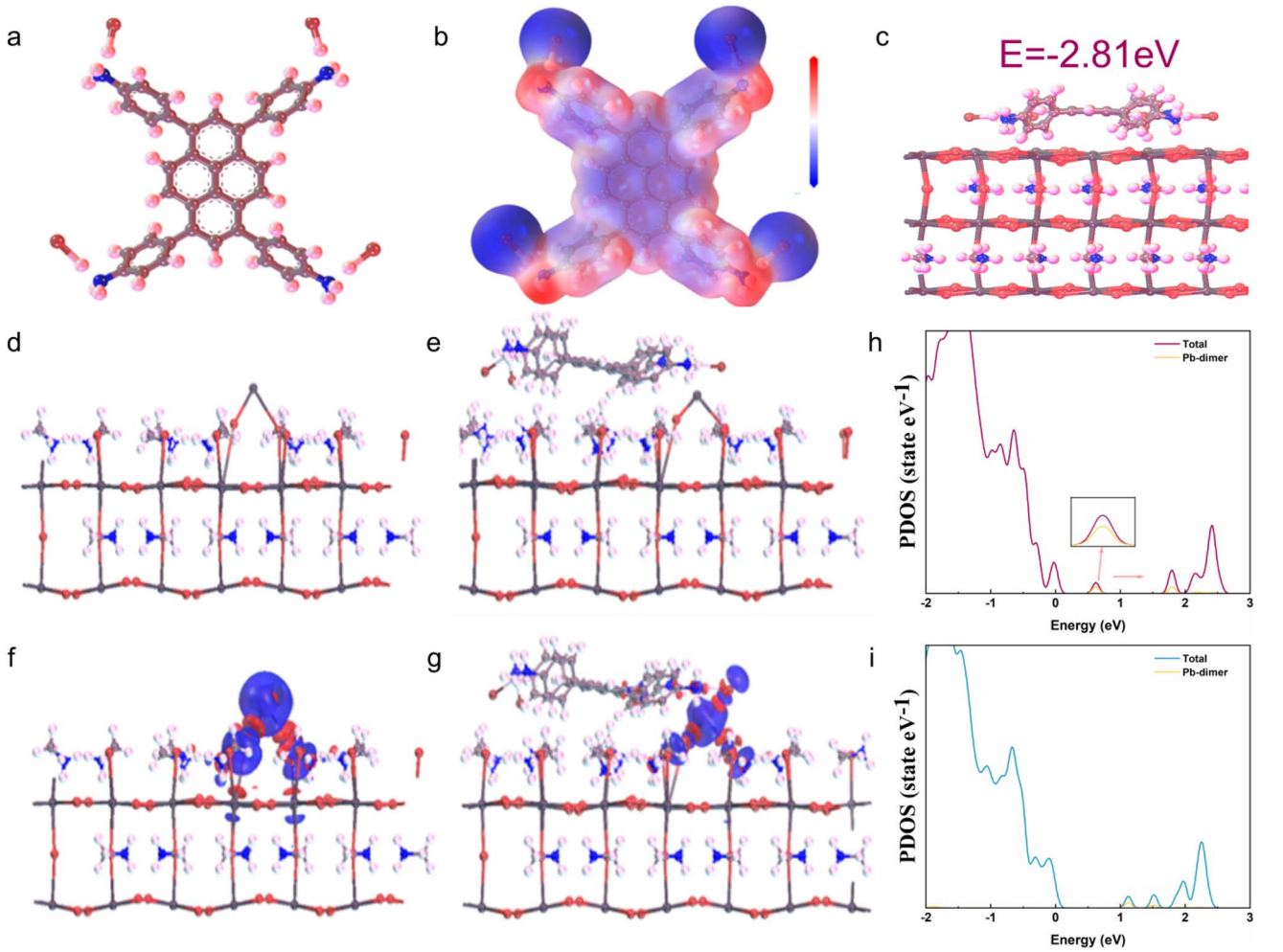

Fig. 2 Theoretical calculations. (a) Optimized spatial configuration of TAPPyI; (b) surface electrostatic potential map of TAPPyI; (c) 3D model of TAPPyI on the perovskite surface; (d) schematic diagram of the structure of the Pb–Pb dimer defect on the perovskite surface; (e) schematic diagram of TAPPyI passivating the Pb–Pb dimer defect; (f) differential charge map of the Pb–Pb dimer defect on the perovskite surface; (g) differential charge map of TAPPyI passivating the Pb–Pb dimer defect, where red and blue represent charge accumulation and depletion, respectively; (h) partial density of states (PDOS) diagram of the Pb–Pb dimer defect; (i) PDOS diagram of TAPPyI passivating the Pb–Pb dimer defect.

between the four aromatic ammonium groups on TAPPyI and Pb^{2+}.[18]

The changes in perovskite defect states and carrier lifetime in perovskite films before and after the introduction of TAPPyI can be understood through PL and TRPL tests. As shown in Fig. 3b, compared to the reference perovskite film, the PL fluorescence peak of the perovskite film treated with TAPPyI is stronger, indicating effective suppression of non-radiative recombination of charge carriers, thereby reducing the number of defect states in the perovskite film. Additionally, compared to the reference perovskite film, the PL fluorescence peak of the perovskite film treated with TAPPyI has undergone a blue shift caused by the passivation on the uncoordinated Pb^{2+} defects of TAPPyI, which is favorable for enhancing the open-circuit voltage (V_{oc}) and improving the PSC performance. The TRPL results further confirm this conclusion, as shown in Fig. 3c, where the carrier lifetime decay trend of the reference perovskite film is more pronounced. The decay curves are fitted using a biexponential model with fast (τ_1) and slow (τ_2) components to calculate the average lifetime of carriers in the perovskite film, corresponding to the transport and recombination of interfacial carriers, as shown in formula (1).

$$y = A_1 \exp\left(-\frac{t}{\tau_1}\right) + A_2 \exp\left(-\frac{t}{\tau_2}\right) + y_0 \quad (1)$$

where A_i and τ_i ($i = 1, 2$) represent the decay amplitude and decay time components, respectively, and detailed lifetime parameters are shown in Table S1.† Subsequently, the corresponding parameters obtained from fitting the double exponential model are input into the calculation formula for the average PL lifetime (τ_{ave}), as shown in formula (2), to obtain the average lifetime of carriers at the interface of the film.

$$\tau_{ave} = \frac{A_1\tau_1^2 + A_2\tau_2^2}{A_1\tau_1 + A_2\tau_2} \quad (2)$$

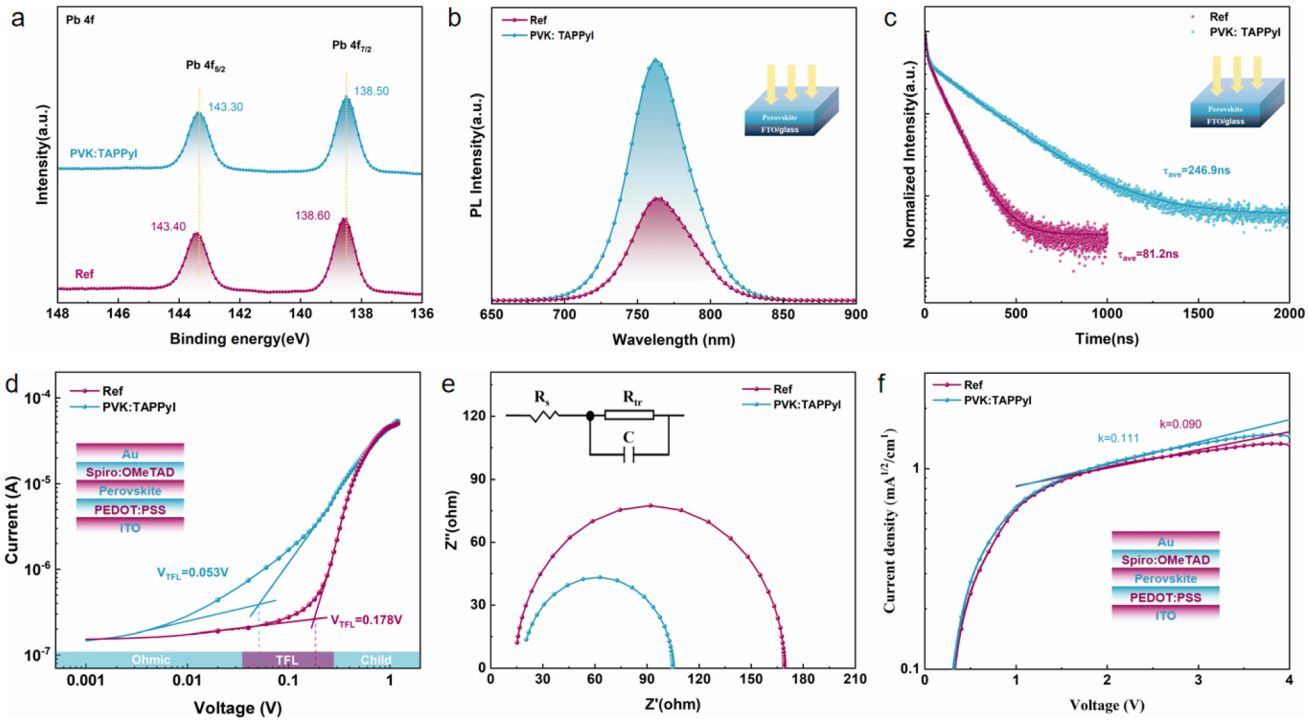

Fig. 3 (a) Characteristic peaks of Pb 4f in the X-ray photoelectron spectroscopy (XPS) spectra of perovskite films before and after modification; (b) steady-state photoluminescence (PL) spectra; (c) time-resolved photoluminescence (TRPL) spectra of perovskite films before and after modification; (d) defect density of hole-only devices before and after modification measured by the space-charge-limited current (SCLC) method; (e) EIS impedance spectra of devices before and after modification under 1.5 G standard solar illumination; (f) hole mobility of devices before and after modification measured by the SCLC method.

The average carrier lifetime in the reference perovskite film is calculated to be 81.2 ns, while it significantly increases to 246.9 ns after modifying the perovskite film with TAPPyI, which implies that the perovskite film with TAPPyI has a lower density of defect states, making it difficult for charge carriers to be captured by defect centers during the transport process. The results show that TAPPyI can effectively passivate the defect states of the perovskite, significantly reduce the non-radiative recombination centers, and thus improve the carrier lifetime, which means higher V_{oc}, FF and PCE in PSC with TAPPyI.

To quantify the defect densities of the perovskite film before and after TAPPyI modification, space-charge-limited current (SCLC) measurements were conducted. Hole-only devices with an FTO/PEDOT:PSS/PVK/Spiro-OMeTAD/Au structure and electron-only devices with an FTO/SnO_2/PVK/PCBM/Au structure were prepared for testing, as shown in Fig. 3d and S9.† The corresponding defect density (N_{trap}) was calculated using formula (3).

$$V_{TFL} = \frac{eN_{trap}L^2}{2\varepsilon\varepsilon_0} \quad (3)$$

where ε_0 is the vacuum permittivity, ε_r is the relative permittivity, V_{TFL} is the trap-filled limit voltage, e is the elementary charge, and L is the film thickness. After calculation, the defect densities of the reference device and the hole-only device with TAPPyI are 1.97×10^{15} and 5.86×10^{14} cm^{-3}, respectively. The defect densities of the electron-only devices are 4.88×10^{15} and 1.97×10^{15} cm^{-3}, respectively. These results indicate that TAPPyI has a significant effect on passivating defects in the perovskite, consistent with the expected outcomes.

Electrochemical impedance spectroscopy (EIS) is often used to analyze the carrier transport characteristics in PSCs. As shown in Fig. 3e, under AM 1.5 G solar illumination, the TAPPyI-modified PSC exhibits a lower transport resistance (R_{tr}) compared to the reference PSCs. Meanwhile, in a dark environment, the recombination resistance (R_{rec}) of the TAPPyI-modified PSC is significantly increased (Fig. S10†). These indicate that the TAPPyI-modified PSC effectively suppresses carrier recombination and exhibits more effective charge transport, thereby further improving the FF and PCE.

The charge transport capability also reflects the carrier mobility. So, hole-only devices with an FTO/PEDOT:PSS/PVK/Spiro/Au structure and electron-only devices with an FTO/SnO_2/PVK/PCBM/Au structure were prepared for measuring the carrier mobility using the space-charge-limited current (SCLC) method. The SCLC voltage–current relationship was tested in a dark environment, and a linear fit was performed for 1.5–3.0 V to obtain the slope (k), as shown in Fig. 3f and S11.† The calculation of mobility is shown in formulae (4) and (5).

$$J = \frac{9\varepsilon_0\varepsilon_r\mu V_{eff}^2}{8L^3} \quad (4)$$

$$\mu = \frac{8000L^3k^2}{9\varepsilon_0\varepsilon_r} \quad (5)$$

where J represents the measured current density, L is the film thickness, μ is the mobility, ε_0 is the vacuum permittivity, ε_r is the relative permittivity, and V_{eff} is the difference between the applied voltage (V_{app}) and the bias voltage (V_{bi}). The hole mobility in the device modified with TAPPyI is 1.60×10^{-4} cm^2 V^{-1} s^{-1}, which is significantly higher than that of the reference device (1.05×10^{-4} cm^2 V^{-1} s^{-1}). Meanwhile, the electron mobility in the device modified with TAPPyI is 1.76×10^{-3} cm^2 V^{-1} s^{-1}, which is also significantly higher than that of the reference device (9.74×10^{-4} cm^2 V^{-1} s^{-1}). It is evident that the device modified with TAPPyI exhibits a significant enhancement in both electron and hole mobility, indicating that the 2D/3D heterostructured perovskite formed by TAPPyI can improve the charge transfer ability of 3D perovskite.

To validate the effect of the 2D/3D heterostructured perovskite formed by TAPPyI on the photovoltaic performances of PSCs, a complete PSC device with an FTO/TiO_2/PVK:TAPPyI/Spiro-OMeTAD/Au structure was fabricated and the cross-section of the entire PSC is shown in Fig. 1c. Furthermore, the J–V curves of the PSCs under reverse scan were recorded under AM 1.5 G solar illumination. Initially, the optimal concentration of TAPPyI in the perovskite precursor solution was explored. As shown in Fig. 4a and Table S2,† as the concentration of TAPPyI increases, the PCE values of the PSCs initially increase and then decrease. When the concentration of TAPPyI is 0.50 mg mL^{-1}, the PSC achieves the best PCE of 22.73% with an open-circuit voltage (V_{oc}) of 1.194 V, a short-circuit current density (J_{sc}) of 24.63 mA cm^{-2} and a FF of 0.773. Meanwhile, the reference PSC without TAPPyI obtains a PCE of 20.51% with a V_{oc} of 1.143 V, a J_{sc} of 24.32 mA cm^{-2}, and a FF of 0.738.

The statistical photovoltaic parameter distributions of the TAPPyI-modified PSCs and reference PSCs are collected in Fig. 4b. Obviously, the TAPPyI-modified PSCs show higher V_{oc}, J_{sc}, FF, and PCE and better reproducibility. It is worth noting that the enhancement in the photovoltaic parameters of TAPPyI-modified PSCs can be primarily attributed to two factors. Firstly, TAPPyI can passivate defects, significantly reduce defect density, reduce non-radiative recombination of charge carriers, and extend carrier lifetime, thereby improving V_{oc} and FF. Secondly, TAPPyI helps with the crystallization of the perovskite, optimizing the film quality of the perovskite layer, enhancing the light-harvesting capacity of the perovskite layer, and thus leading to higher J_{sc}. The external quantum efficiency (EQE) spectra were recorded to examine the accuracy of the J_{sc} of PSCs, as shown in Fig. 4c. Both PSCs exhibit similar spectral responses, and the EQE of the TAPPyI-modified PSC is higher than that of the reference PSC in the range of 350–720 nm, which is due to the enhanced light-harvesting capacity and charge transfer ability of the 2D/3D heterostructured perovskite formed by TAPPyI. The integrated current densities of the TAPPyI-modified PSC and reference PSC calculated from the EQE spectra are 23.11 mA cm^{-2} and 22.30 mA cm^{-2}, respectively. It should be noted that the integrated current densities are slightly lower than the J_{sc} obtained in J–V

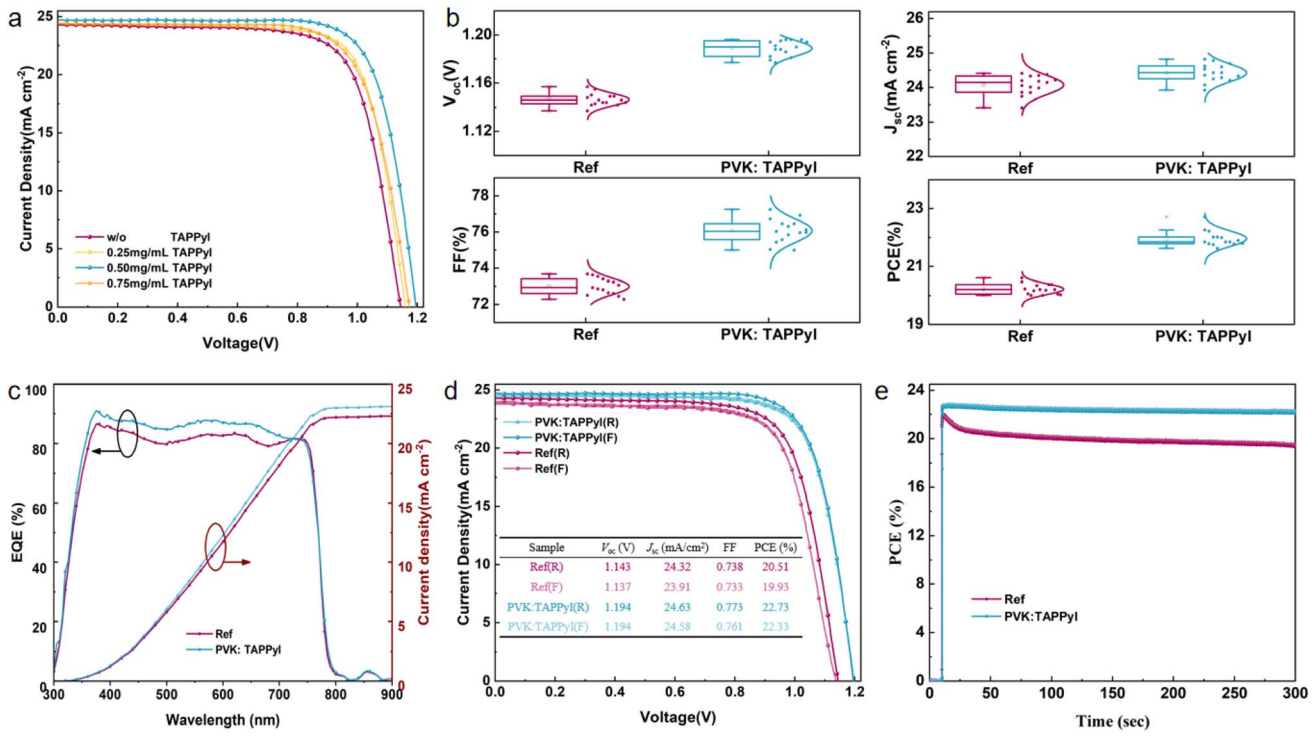

Fig. 4 Photovoltaic performances of the PSCs. (a) Best J–V reverse scan curves of the PSCs with different TAPPyI doping concentrations; (b) statistical distributions of V_{oc}, J_{sc}, FF and PCE of the PSCs; (c) EQE curves and integrated current densities of the PSCs; (d) best J–V curves of the PSCs under forward and reverse scans and the corresponding PV parameter statistics table; (e) the steady-state PCE output of the PSCs at the maximum power point.

measurements, which is mainly due to EQE measurements being conducted at a single wavelength, where the intensity is much lower than the intensity of full-spectrum irradiation. We also recorded the *J–V* curves of the PSCs under forward and reverse scans to assess hysteresis behavior in Fig. 4d. Compared to the reference PSC, the TAPPyI-modified PSC has a smaller hysteresis. Additionally, the steady-state PCE value at the maximum power point under continuous 1 sun illumination is shown in Fig. 4e. Compared with the reference PSC, the TAPPyI-modified PSC has faster photoelectric response and more stable output capability.

Stability is a crucial factor in evaluating the performance of the PSCs, and the stability of the PSCs is closely related to the stability of perovskite films. Next, we first investigated the influence of TAPPyI on the stability of perovskite films. As shown in the inset of Fig. 5d, the water contact angle of the TAPPyI-modified perovskite film was 98.45°, while that of the reference perovskite film is only 63.09°. When a water droplet was placed on the reference perovskite film, the film was immediately destroyed, producing yellow PbI_2. However, the TAPPyI-modified perovskite film was not broken when the water droplet was placed on it for 10 seconds (Fig. S12†). Fig. S13† shows the photos of the perovskite films before and after aging in an environment of 85 °C under a N_2 atmosphere for 360 hours. After aging, the color of the reference perovskite film begins to turn yellow and gradually deepens, which is due to the formation of PbI_2 by the destruction of the perovskite. However, the TAPPyI-modified perovskite film was relatively stable and no significant color change was observed. In addition, the SEM images of perovskite films after aging in an environment of 85 °C and 85% humidity for 360 hours are shown in Fig. 5a. The surface of the reference perovskite film shows blurred grain boundaries, pores, and white particles, which are due to the precipitation and aggregation of PbI_2, leading to the aggregation of water molecules, and the easy escape of cations from the perovskite film under moisture and heating conditions. In contrast, the TAPPyI-modified perovskite film exhibits a uniform surface, clear grains and no white particles after aging. Furthermore, from the photos of the PSCs before and after aging in an environment of 85 °C and 85% humidity for 360 hours in Fig. 5b, it can be observed that the perovskite film in the reference PSC significantly fades after aging, while the color change of the perovskite film in the TAPPyI-modified PSC is very small. Fig. 5c shows the XRD patterns of the perovskite films after aging in an environment of 85 °C and 85% humidity for 360 hours. The reference perovskite film showed a strong PbI_2 peak, indicating that the perovskite has undergone degradation, producing PbI_2. However, the PbI_2 peak of the TAPPyI-modified perovskite film is still weak, and there is no significant change in the 2D perovskite peak. The above results indicate that the TAPPyI-modified perovskite film exhibits high moisture and heat stability, which is due to the following reasons: Firstly, the TAPPyI can passivate the defects of the perovskite film and reduce active sites. Secondly, the interaction between the four terminal aryl ammonium groups of the TAPPyI and the perovskite layer through ionic and hydrogen bonds

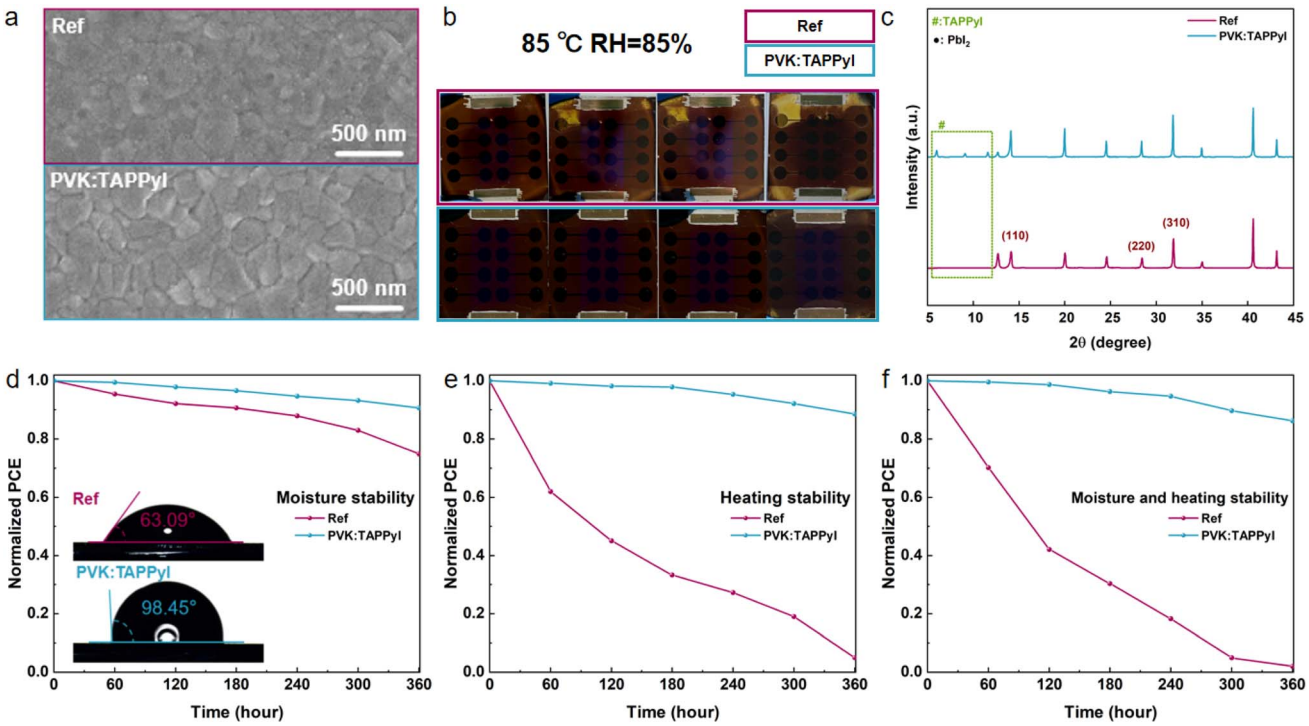

Fig. 5 Stability testing of the PSCs. (a) SEM images of the perovskite films aged at 85 °C and 85% humidity for 360 hours; (b) changes on the backside of the PSCs aged at 85 °C and 85% humidity for 360 hours; (c) XRD patterns of the perovskite films aged at 85 °C and 85% humidity for 360 hours; (d) moisture stability of the PSCs at room temperature with 85% humidity and water contact angles of the perovskite films; (e) heat stability of the PSCs at 85 °C in a N_2 environment; (f) overall moisture and heat stability of the PSCs at 85 °C with 85% humidity.

exposes the hydrophobic pyrene groups and aromatic rings on the crystal surface. Thirdly, the TAPPyI can effectively fix $[PbI_6]^{4-}$ together to suppress the migration of cations such as MA^+ and FA^+, further ensuring the structural stability of the perovskite. Lastly, the introduction of TAPPyI leads to larger grains and denser grain boundaries in the perovskite film and forms a more stable 2D structure.

As mentioned above, the TAPPyI-modified perovskite film has high stability against moisture and heating. Then the moisture and heating stabilities of the PSCs based on the TAPPyI-modified perovskite film in different environments were studied. Firstly, the moisture stability of the PSCs was tested at room temperature with a relative humidity of 85%. As shown in Fig. 5d, after 360 hours of aging, the PCE of the TAPPyI-modified PSC still remained at 90.7% of its initial value, while the PCE of the reference PSC retained only 74.9% of its initial value. In addition, we also studied the heat stability of the PSCs at 85 °C under a N_2 atmosphere. In Fig. 5e, compared to the reference PSC, the heat stability of the TAPPyI-modified PSC was significantly improved, retaining 88.6% of the initial PCE after 360 hours of aging at 85 °C under a N_2 atmosphere. Furthermore, in order to evaluate the overall stability of the PSCs against moisture and heating, the PSCs were aged in an environment of 85 °C and 85% humidity (ISOS-D-3). As shown in Fig. 5f, after 360 hours of aging, the reference PSC lost more than 98% of the initial PCE, whereas the TAPPyI-modified PSC lost only about 14% of the initial PCE. The above studies demonstrate that the PSCs with the 2D/3D heterostructured perovskite formed by TAPPyI indeed exhibit high resistance to moisture and heating under different aging conditions, which is consistent with the stability results of the TAPPyI-modified perovskite film.

3. Conclusion

In summary, in order to enhance the moisture and heat stability of the PSCs, a new pyreneammonium iodide TAPPyI is introduced into 3D perovskite precursor solution for forming a 2D/3D heterostructured perovskite. The quality of the 2D/3D heterostructured perovskite film has been significantly improved, increasing grain size while making the surface denser and smoother. Due to the hydrophobicity of the pyrene and aromatic ring of TAPPyI, the passivation of perovskite defects by TAPPyI, and the formation of a more stable 2D/3D heterostructured perovskite film, the TAPPyI-modified perovskite film exhibits high moisture and heat stability, effectively preventing the escape of cations and film degradation. In addition, the planar nature of the pyrene group ensures good charge transport performance, and the iodide with aromatic amine side groups effectively passivates Pb^{2+} defects and compensates for halide vacancies, reducing defects and non-radiative recombination, thereby extending carrier lifetime and improving charge transport ability. Finally, compared to the reference PSC, the performance of the TAPPyI-modified PSC was significantly improved, with PCE increasing from 20.51% to 22.73%. At the same time, the stability of the TAPPyI modified PSC was greatly improved, retaining 86% of the initial PCE after 360 hours in an environment of 85 °C and 85% humidity (ISOS-D-3), while the reference PSC retained only 2%. This work demonstrates the feasibility of using a conjugated planar molecule as a 2D cation to construct a 2D/3D heterostructured perovskite for improving the PCE and the stability of PSCs.

Data availability

The data that support the findings of this study are available in the ESI.†

Author contributions

Z. Wan conceived the idea for the project. Y. Wang and H. Lu fabricated and characterized the devices. R. Wei and H. Yin performed and discussed the DFT calculations. H. Zeng participated in the characterization of other properties. Z. Wan, Y. Wang and H. Lu analyzed all data and wrote the manuscript. M. Azam contributed to refining the language. Z. Wan and Y. Wang contributed to revising the manuscript. Z. Wan, J. Luo and C. Jia directed and supervised the project. All authors discussed the results and commented on the manuscript.

Conflicts of interest

The authors declare no conflict of interest.

Acknowledgements

The authors are grateful to the National Natural Science Foundation of China (62374029, 22175029 and 62104031), the Natural Science Foundation of Shenzhen Innovation Committee (JCYJ20210324135614040), the Technical Field Funds of 173 Project (2021-JCJQ-JJ-0663) and the Fundamental Research Funds for the Central Universities of China (ZYGX2021J010 and Y030202059018023) for financial support.

References

1 H. R. Tan, A. Jain, O. Voznyy, X. Z. Lan, F. P. G. de Arquer, J. Z. Fan, R. Quintero-Bermudez, M. J. Yuan, B. Zhang, Y. C. Zhao, F. J. Fan, P. C. Li, L. N. Quan, Y. B. Zhao, Z. H. Lu, Z. Y. Yang, S. Hoogland and E. H. Sargent, *Science*, 2017, **355**, 722.

2 X. P. Zheng, B. Chen, J. Dai, Y. J. Fang, Y. Bai, Y. Z. Lin, H. T. Wei, X. C. Zeng and J. S. Huang, *Nat. Energy*, 2017, **2**, 17102.

3 H. X. Dang, K. Wang, M. Ghasemi, M. C. Tang, M. De Bastiani, E. Aydin, E. Dauzon, D. Barrit, J. Peng, D. M. Smilgies, S. De Wolf and A. Amassian, *Joule*, 2019, **3**, 1746.

4 T. J. Jacobsson, J. P. Correa-Baen, M. Pazoki, M. Saliba, K. Schenk, M. Grätzel and A. Hagfeldt, *Energy Environ. Sci.*, 2016, **9**, 1706.

5 Y. Zhao, F. Ma, Z. H. Qu, S. Q. Yu, T. Shen, H. X. Deng, X. B. Chu, X. X. Peng, Y. B. Yuan, X. W. Zhang and J. B. You, *Science*, 2022, **377**, 531.

6 J. S. Luo, B. W. Liu, H. M. Yin, X. Zhou, M. J. Wu, H. Y. Shi, J. Y. Zhang, J. Elia, K. C. Zhang, J. C. Wu, Z. Q. Xie, C. Liu, J. Y. Yuan, Z. Q. Wan, T. Heumueller, L. Lüer, E. Spiecker, N. Li, C. Y. Jia, C. J. Brabec and Y. C. Zhao, *Nat. Commun.*, 2024, **15**, 2002.

7 (*a*) A. Abate, M. Saliba, D. J. Hollman, S. D. Stranks, K. Wojciechowski, R. Avolio, G. Grancini, A. Petrozza and H. J. Snaith, *Nano Lett.*, 2014, **14**, 3247; (*b*) F. Matteocci, Y. Busby, J. J. Pireaux, G. Divitini, S. Cacovich, C. Ducati and A. Di Carlo, *ACS Appl. Mater. Interfaces*, 2015, **7**, 26176; (*c*) T. Q. Niu, J. Lu, R. Munir, J. B. Li, D. Barrit, X. Zhang, H. L. Hu, Z. Yang, A. Amassian, K. Zhao and S. Z. Liu, *Adv. Mater.*, 2018, **30**, 1706576.

8 (*a*) T. Zhao, C. C. Chueh, Q. Chen, A. Rajagopal and A. K. Y. Jen, *ACS Energy Lett.*, 2016, **1**, 757; (*b*) Y. X. Zong, Z. M. Zhou, M. Chen, N. P. Padture and Y. Y. Zhou, *Adv. Energy Mater.*, 2018, **8**, 1800997; (*c*) N. Aristidou, C. Eames, I. Sanchez-Molina, X. N. Bu, J. Kosco, M. S. Islam and S. A. Haque, *Nat. Commun.*, 2017, **8**, 15218.

9 N. Ali, S. Rauf, W. G. Kong, S. Ali, X. Y. Wang, A. Khesro, C. P. Yang, B. Zhu and H. Z. Wu, *Renewable Sustainable Energy Rev.*, 2019, **109**, 160.

10 J. Cao, X. D. Lv, X. X. Feng, R. Q. Meng, Y. Y. Wu and Y. Tang, *J. Am. Chem. Soc.*, 2018, **140**, 11577.

11 (*a*) J. C. Blancon, H. Tsai, W. Nie, C. C. Stoumpos, L. Pedesseau, C. Katan, M. Kepenekian, C. M. M. Soe, K. Appavoo, M. Y. Sfeir, S. Tretiak, P. M. Ajayan, M. G. Kanatzidis, J. Even, J. J. Crochet and A. D. Mohite, *Science*, 2017, **355**, 1288; (*b*) Y. N. Chen, Y. Sun, J. J. Peng, W. Zhang, X. J. Su, K. B. Zheng, T. Pullerits and Z. Q. Liang, *Adv. Energy Mater.*, 2017, **7**, 1700162; (*c*) J. F. Lu, L. C. Jiang, W. Li, F. Li, N. K. Pai, A. D. Scully, C. M. Tsai, U. Bach, A. N. Simonov, Y. B. Cheng and L. Spiccia, *Adv. Energy Mater.*, 2017, **7**, 1700444; (*d*) L. Ma, J. Dai and X. C. Zeng, *Adv. Energy Mater.*, 2017, **7**, 1601731; (*e*) C. C. Stoumpos, C. M. M. Soe, H. Tsai, W. Y. Nie, J. C. Blancon, D. Y. H. Cao, F. Z. Liu, B. Traoré, C. Katan, J. Even, A. D. Mohite and M. G. Kanatzidis, *Chem*, 2017, **2**, 427.

12 (*a*) R. T. Wang, T. G. Sun, T. Wu, Z. Q. Zhu, J. Y. Shao, Y. W. Zhong and Y. Hua, *Chem. Eng. J.*, 2022, **430**, 133065; (*b*) F. Yang, P. T. Zhang, M. A. Kamarudin, G. Kapil, T. L. Ma and S. Hayase, *Adv. Funct. Mater.*, 2018, **28**, 1804856.

13 T. M. Koh, V. Shanmugam, J. Schlipf, L. Oesinghaus, P. Müller-Buschbaum, N. Ramakrishnan, V. Swamy, N. Mathews, P. P. Boix and S. G. Mhaisalkar, *Adv. Mater.*, 2016, **28**, 3653.

14 (*a*) X. L. Sun, X. Deng, Z. Li, B. J. Xiong, C. Zhong, Z. L. Zhu, Z. A. Li and A. K. Y. Jen, *Adv. Sci.*, 2020, **7**, 1903331; (*b*) X. L. Sun, Q. F. Xue, Z. L. Zhu, Q. Xiao, K. Jiang, H. L. Yip, H. Yan and Z. A. Li, *Chem. Sci.*, 2018, **9**, 2698.

15 (*a*) T. V. Dubinina, E. O. Moiseeva, D. A. Astvatsaturov, N. E. Borisova, P. A. Tarakanov, S. A. Trashin, K. De Wael and L. G. Tomilova, *New J. Chem.*, 2020, **44**, 7849; (*b*) P. P. Dash, P. Mohanty, S. Behera, R. Behura, B. B. Palai, B. Nath, S. K. Sahoo and B. R. Jali, *Methods*, 2023, **219**, 127; (*c*) Y. Li, C. Zhang, P. Y. Gu, Z. L. Wang, Z. Q. Li, H. Li, J. M. Lu and Q. C. Zhang, *Chem.–Eur. J.*, 2018, **24**, 7845.

16 (*a*) K. S. Kim, Y. Zhao, H. Jang, S. Y. Lee, J. M. Kim, K. S. Kim, J. H. Ahn, P. Kim, J. Y. Choi and B. H. Hong, *Nature*, 2009, **457**, 706; (*b*) F. Yang, M. A. Kamarudin, P. T. Zhang, G. Kapil, T. L. Ma and S. Hayase, *ChemSusChem*, 2018, **11**, 2348; (*c*) J. Y. Shao, B. C. Yu, Y. D. Wang, Z. R. Lan, D. M. Li, Q. B. Meng and Y. W. Zhong, *ACS Appl. Energy Mater.*, 2020, **3**, 5058; (*d*) M. G. Kaplunov, I. K. Yakushchenko, S. S. Krasnikova and S. B. Echmaev, *Mendeleev Commun.*, 2016, **26**, 437; (*e*) J. P. Mora- Fuentes, D. Cortizo-Lacalle, S. Collavini, K. Strutynski, W. R. Tress, M. Saliba, S. M. Zakeeruddin, I. Kosta, M. Melle-Franco, M. Grätzel, J. L. Delgado and A. Mateo-Alonso, *J. Mater. Chem. C*, 2019, **7**, 4332; (*f*) J. Salunke, A. Singh, D. X. He, H. D. Pham, Y. Bai, L. Z. Wang, S. Dahlström, M. Nyman, S. Manzhos, K. Feron, R. Österbacka, A. Priimagi, P. Vivo and P. Sonar, *Org. Electron.*, 2020, **77**, 105524.

17 (*a*) L. Z. Zhang, C. Liu, J. Zhang, X. N. Li, C. Cheng, Y. Q. Tian, A. K. Y. Jen and B. M. Xu, *Adv. Mater.*, 2018, **30**, 1804028; (*b*) D. Li, C. Sun, H. Li, H. Shi, X. X. Shai, Q. Sun, J. B. Han, Y. Shen, H. L. Yip, F. Huang and M. K. Wang, *Chem. Sci.*, 2017, **8**, 4587.

18 M. N. Hou, Y. Z. Xu, B. Zhou, Y. Tian, Y. Wu, D. K. Zhang, G. C. Wang, B. Z. Li, H. Z. Ren, Y. L. Li, Q. Huang, Y. Ding, Y. Zhao, X. D. Zhang and G. F. Hou, *Adv. Funct. Mater.*, 2020, **30**, 2002366.